


# Photoinduced control of ferroelectricity in hybrid-improper ferroelectric superlattices

Lingyuan Gao<sup>1</sup>, Charles Paillard<sup>2</sup>, and Laurent Bellaïche<sup>1</sup>

<sup>1</sup>Physics Department and Institute for Nanoscience and Engineering, University of Arkansas, Fayetteville, Arkansas 72701, USA

<sup>2</sup>Université Paris-Saclay, CentraleSupélec, CNRS, Laboratoire SPMS, 91190 Gif-sur-Yvette, France

 (Received 27 June 2022; revised 21 January 2023; accepted 1 March 2023; published 29 March 2023)

We reveal a photoinduced control of ferroelectricity in hybrid-improper ferroelectric superlattices, using *ab initio* theory. Along with a notable photostriction effect, thermalized carriers from photoexcitation affect octahedral tiltings along different directions. A trilinear coupling between antipolar and tilting modes drives corresponding cationic displacements, and this results in a decrease in polarization under light. Together with recent experimental evidence, our study therefore demonstrates that light is a viable route to engineer functionalities in materials.

DOI: [10.1103/PhysRevB.107.104109](https://doi.org/10.1103/PhysRevB.107.104109)

## I. INTRODUCTION

With spontaneous and switchable electric polarizations, ferroelectrics (FEs) have important implications not only in fundamental science but also in device applications. Conventional ferroelectricity, such as in perovskite oxides  $\text{BaTiO}_3$ , is attributed to a  $p$ - $d$  hybridization between Ti  $d^0$  and oxygen  $p$  states, where the long-range Coulomb forces are favored against the short-range repulsion [1]. As a result, Ti off-centering displacement in  $\text{BaTiO}_3$  is induced, which breaks the centrosymmetry. With a different origin, the “hybrid improper” ferroelectricity, identified in perovskite superlattices such as  $\text{ABO}_3/\text{A}'\text{BO}_3$  and layered perovskites  $(\text{ABO}_3)_2(\text{AO})$  [2–4], arises from a trilinear coupling between a polar mode on  $A$  sites and two nonpolar tilting modes of  $\text{BO}_6$  octahedra. The mechanism relies more on the geometry of the lattice (namely, the nonfull compensation between antipolar displacements of  $A$  cations on different layers) rather than on the electrostatic forces as in conventional FEs [5,6].

Different approaches have been proposed to manipulate ferroelectricity. Strains applied on thin films can affect the electric polarization of  $\text{BaTiO}_3$ , and can also render the quantum paraelectric  $\text{SrTiO}_3$  ferroelectric and even increase its transition temperature [7,8]. Charge doping has been demonstrated to be another effective manner to tune ferroelectricity and create novel phases. In conventional FEs such as  $\text{LiNbO}_3$  and  $\text{BaTiO}_3$ , the ferroelectric displacement can be suppressed by increasing the number of doped carriers [9–12], while in the trilinear Ruddlesden-Popper phase of layered perovskites, a very recent study shows that in  $\text{A}_3\text{Sn}_2\text{O}_7$  electrostatic doping leads to an increase of octahedral rotation [13], which then enhances the polarization. Since carriers can screen the long-range interaction and have a tendency to preserve the centrosymmetry, it is counterintuitive that ferroelectricity coexists with metallicity. Such unusual coexistence had not been discovered until 2013, when  $\text{LiOsO}_3$  was identified as the first “polar metal” [14]—six decades after its theoretical prediction [15]. More recent works show that the 2D topological semimetal  $\text{WTe}_2$  also displays a switchable polarization [16].

Alternatively, with the advancement of optical pumping, intense irradiation by ultrafast laser pulses has become another method to trigger novel phase transitions. It is not only limited to the low-frequency or THz dynamical process where phonons are resonantly excited to drive the system [17–20]. By absorbing photons, photoexcited electrons at quasiequilibrium condition can reshape the potential energy landscape and induce structural distortions, which are rarely visited otherwise. Photoinduced phase transitions have been predicted [21] and realized in FEs [22]; recently, it has been revealed that optical excitation can induce an increasing octahedral tilting in Ca-doped  $\text{SrTiO}_3$  and  $\text{EuTiO}_3$  [23,24]. Charge-ordered phases can also form after the illumination of light in  $\text{LaTe}_3$ ,  $\text{MoTe}_2$ , and  $\text{WTe}_2$  [25,26].

In this work, using first-principles calculations to simulate the effect of photoexcited carriers, we show the pivotal role of light illumination in controlling the electric polarization of hybrid-improper ferroelectrics (HIFs). Intuitively, photoexcited carriers should screen the electric polarization as a response to the intrinsic electric field. Instead in HIFs, at quasiequilibrium state, photoexcited carriers tailor the polarization by governing tilting modes of octahedra via trilinear coupling [2–4]. This is in contrast to electrostatic doping in conventional FEs, where carriers screen the long-range Coulomb force and reduce the ferroelectric off-centering displacement [10,11]. As an example, by choosing the prototypical HIF superlattice  $\text{LaGaO}_3/\text{YGaO}_3$ , we show how tiltings increase and antipolar displacements concomitantly get enhanced, but polarization decreases with the intensity of illumination. This is because though light causes larger displacements of La and Y as a result of the enhancement of tiltings, the two cations move antiparallel to each other. As the magnitudes of their individual displacements become closer with larger concentration on photoexcited carriers, the net polarization decreases. This is different from  $\text{PbTiO}_3$ , where the polar instability is directly suppressed while the tilting instabilities are directly enhanced under photoillumination [21]. The polarization change occurs concurrently with a photoinduced volume expansion, known as the photostriction effect [27–29].

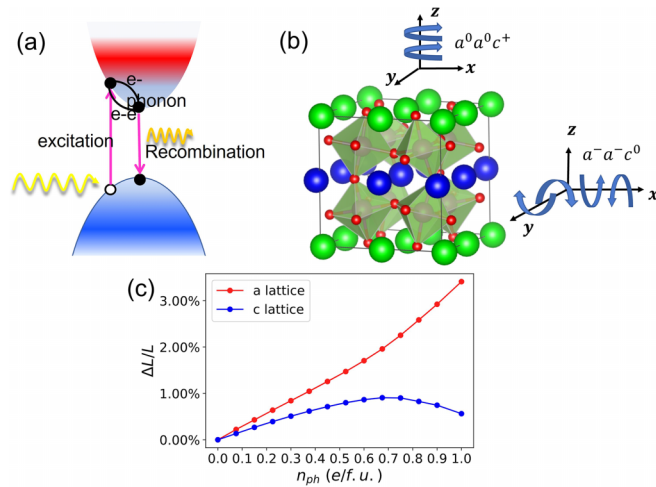


FIG. 1. (a) Three dynamic events electrons experience after illumination, including photoexcitation, electron-electron/electron-phonon interaction, and electron-hole recombination. (b) Illustration about out-of-plane, in-phase tilting  $c^+$  and in-plane, out-of-phase tilting  $a^-$  in LaGaO<sub>3</sub>/YGaO<sub>3</sub>. Two arrows indicate tilting directions of octahedra in front and rear layers around respective axis, respectively. (c) Photoinduced strain for in-plane  $a$  and out-of-plane  $c$  lattice constants as a function of photoexcited carriers  $n_{ph}$ .

## II. METHODOLOGY

When an insulator is irradiated by above-band-gap photons, dynamics of excited carriers can be divided into three stages: photoexcitation, thermalization, and recombination [30,31]. By absorbing photon energy, electrons are pumped to occupy conduction bands and leave holes in valence bands. With electron-electron/hole-hole interaction, two types of carriers will reach quasiequilibrium where the population follows a Fermi-Dirac distribution with well-defined carrier temperatures. The excitation and carrier-carrier interaction happen at a femtosecond timescale [32–34]. Redistributed electrons and holes on conduction bands and valence bands will reshape the potential energy surface, and the restoring forces will drive fast atomic motions [35,36]. It cannot only be resolved in experiments but also can be distinguished from subsequent events such as heat transfer from electrons to lattice due to electron-phonon interaction and phonon decay at a longer timescale [23,36]. The above-mentioned processes still have shorter timescales compared to the recombination process at the nanosecond level [32,37]. All dynamical processes are illustrated in Fig. 1(a). Here we focus on the transient state after photoexcitation and before heat transfer, where carriers have reached quasiequilibrium, and atoms are well relaxed by interatomic forces. This state can be created by a pulsed laser.

This transient state can be described using constrained density functional theory (DFT) calculations [38,39], where the intensity of illumination can be converted to the number of photoexcited electron-hole pairs,  $n_{ph}$ , via

$$\eta J S_0 = \frac{d}{a_0} \Delta_{\text{gap}} n_{ph}. \quad (1)$$

$\eta$  denotes the conversion efficiency while  $J$  denotes the energy fluence of one laser pulse.  $a_0$ ,  $S_0$  denote the out-of-plane

lattice constant and area of one formula unit (f.u.) of the cell, respectively. With  $\Delta_{\text{gap}} = 4$  eV as the indirect band gap predicted by DFT for LaGaO<sub>3</sub>/YGaO<sub>3</sub> (see Fig. S2 in the Supplemental Material (SM) [40]; see also Refs. [41–43] therein), if we take  $\eta = 25\%$  (which is close to photoconversion efficiency of a solar cell), for a thin film with thickness  $d = 10$  nm, the number of photoexcited carriers  $n_{ph}$  is  $0.44$  e/f.u. for a homogeneous illumination of  $J = 10$  mJ/cm<sup>2</sup>—which is accessible for contemporary pulsed lasers. As a sound estimate, we thus vary  $n_{ph}$  in the range of 0–1 e/f.u. Since we are not focusing on carrier dynamics, methods such as time-dependent density functional theory used elsewhere are not considered [23,24].

We adopt the conventional cell containing four superlattice formula units so that the octahedral tilting pattern can be fully displayed [shown in Fig. 1(b)]. With  $a^- a^- c^+$  in Glazer notation [44], the tiltings are out-of-phase along in-plane axes but in-phase along the out-of-plane axis. In the presence of photoexcited carriers, we perform structural relaxation including both atomic coordinates and lattice using the plane-wave DFT code ABINIT [45]. Other details of calculations can be found in the SM [40].

## III. PHOTOSTRICTION AND PHOTOINDUCED POLARIZATION

We first look at the photostriction effect, namely, photoinduced lattice change in LaGaO<sub>3</sub>/YGaO<sub>3</sub>. Figure 1(c) shows that the in-plane lattice constant expands with the injection of photoexcited carriers, and the increase is up to 3.5% when  $n_{ph} = 1$  e/f.u. The out-of-plane lattice constant first increases by 0.9% when  $n_{ph} = 0.7$  e/f.u. and then gradually decreases. A similar effect has been observed in halide perovskites, which has been attributed to the character of electrons excited by photons with different energies [46,47]. Photostriction in the HIF superlattice is much more pronounced than the one predicted by the  $\Delta$ SCF method in BaTiO<sub>3</sub> [28], and with the same order of magnitude as in PbTiO<sub>3</sub> and BiFeO<sub>3</sub> [27,28]. The compressive photoinduced strain in conventional FEs and multiferroics is explained by a converse piezoelectric effect, where screening and resulting reduction of polarization from illumination lead to a shrinking of the lattice constant [27,28]. With a different origin, here we associate the tensile, photoinduced strain in HIFs with a weaker Ga-O bonding and an elongated Ga-O bond length, so as to lower the energy of the bonding and antibonding states occupied by thermalized holes and electrons, respectively (details are provided in the SM [40]).

Polar displacements have been widely used to characterize the ferroelectricity in polar metals and doped systems [10,11,13,48]. As in Ref. [13], the effective polarization  $\bar{P}$  is computed as the sum of atomic displacements from high-symmetry positions times the respective Born effective charges (see the SM for more details [40]). Since we consider a small number of photoexcited carriers, we take the Born effective charges to be the same before and after illumination. Figure 2(a) shows the variation of the total polarization,  $P$ , with  $n_{ph}$ .  $P$  decreases linearly before the turning point  $n_{ph} = 0.6$  e/f.u., at which the out-of-plane lattice constant also changes its behavior as shown in Fig. 1(c). After that,  $P$

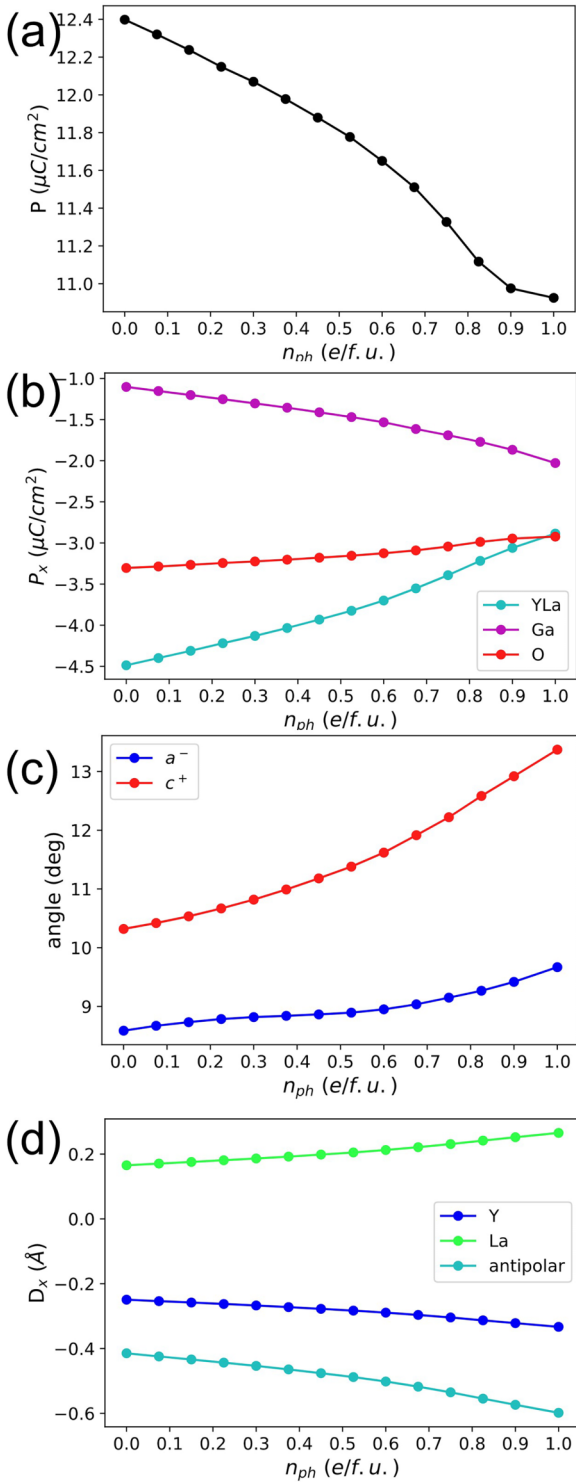


FIG. 2. Variations of different quantities with the number of photoexcited carriers  $n_{ph}$ . (a) Magnitude of polarization  $P$ . (b)  $P_x$  component contributed by  $A$ -site cations La and Y, Ga, and oxygens, respectively. (c) The out-of-phase tilting ( $a^-$ ) angle and in-phase tilting ( $c^+$ ) angle. (d) The in-plane ionic displacement  $D_x^Y$ ,  $D_x^{La}$ , and antipolar displacement  $D_x^Y - D_x^{La}$ .

decreases at a more rapid rate. At  $n_{ph} = 1 e/f.u.$ , it arrives at 10.9  $\mu C/cm^2$ , reducing by 12% from its original value. To determine the contribution from each atomic species, we decompose the  $x$  component of the polarization  $P_x$  into  $P_x^{LaY}$ ,

$P_x^{Ga}$ , and  $P_x^O$ , which originate from displacements of cations on the  $A$  site, Ga, and oxygens, respectively. We note that the components of the polarization along the  $x$  and  $y$  directions are almost identical (see Fig. S3 in the SM [40]) and the component along the  $z$  direction  $P_z$  is almost 0, indicating that the total polarization is along the  $[-1-10]$  direction, typical of HIF systems [49,50]. As shown in Fig. 2(b), the polarization in the  $LaGaO_3/YGaO_3$  superlattice is largely contributed by cations on  $A$  sites for the dark condition  $n_{ph} = 0$ . This results from the antipolar displacements between  $\vec{D}_{La}$  and  $\vec{D}_Y$  driven by two unstable nonpolar octahedral tiltings  $a^0a^0c^+$  and  $a^-a^-c^0$  [4], and it constitutes over 50% of the total polarization. With  $\vec{D}_{La} \neq -\vec{D}_Y$ , oxygen displacements at LaO and YO layers related with  $a^-a^-c^0$  tilting are also asymmetric, and that contributes partially to  $P_x$  and  $P_y$  too. By turning on the light,  $P_x^{LaY}$  from the  $A$ -site antipolar mode increases significantly, while  $P_x^{Ga}$  becomes more negative. Overall three contributions therefore give rise to a less negative  $P_x$  and a smaller  $P$  with an increasing  $n_{ph}$ .

To elucidate the origin of the polarization change under illumination, we plot the  $\phi_{a^-}$  antiphase tilting angle and the  $\phi_{c^+}$  in-phase tilting angle as a function of  $n_{ph}$  in Fig. 2(c). We find increase on both  $\phi_{a^-}$  and  $\phi_{c^+}$ , but the increase of  $\phi_{c^+}$  is more remarkable. The tiltings are enhanced by the photoexcited carriers. Nevertheless, in stark contrast to the previously studied layered perovskite  $A_3Sn_2O_7$  with electrostatic doping [13], a large amplitude of tilting here does not imply a larger polarization. This is because previous atomistic theories reveal that the antipolar displacement  $\vec{D}^Y - \vec{D}^{La}$ , rather than the polar displacement  $\vec{D}^Y + \vec{D}^{La}$  (which is directly linked to polarization), is proportional to the product of the two tilting angles [50,51]:

$$D_x^Y - D_x^{La} \propto \phi_{a^-} \phi_{c^+} (K^Y + K^{La}). \quad (2)$$

Here,  $K$  denotes the coupling coefficient between in-plane atomic displacements and tilting modes, and  $K^Y$  and  $K^{La}$  have the same sign. To show this correlation, we plot  $D_x^Y$ ,  $D_x^{La}$  and  $D_x^Y - D_x^{La}$  vs  $n_{ph}$  in Fig. 2(d). Indeed, following enhanced tiltings,  $D_x^Y$  and  $D_x^{La}$  (which are always opposite in sign) both increase in magnitude. Resultantly, the antipolar displacement  $D_x^Y - D_x^{La}$  also increases. This also results in a polarization approximated as

$$P_x \sim D_x^Y + D_x^{La} \propto \phi_{a^-} \phi_{c^+} (K^Y - K^{La}), \quad (3)$$

which shows that apart from tilting amplitudes,  $P$  is also dependent on the coupling difference  $K^Y - K^{La}$ . Due to mutual competition, this coupling difference is more delicate than their sum  $K^Y + K^{La}$ . The smaller  $P_x^{YLa}$  with increasing  $n_{ph}$  suggests that the two coupling strengths come closer to each other with an increasing illumination.

#### IV. PHOTOINDUCED MODE COUPLING

To further understand the coupling between antipolar and nonpolar tilting modes, we study phonons of the highly symmetric  $P4/mmm$  tetragonal cell with one formula unit at different  $n_{ph}$ . The 10-atom,  $P4/mmm$  tetragonal cell is the parent of  $Pmc2_1$  structure (that has 20 atoms in its primitive cell). In combination with different tiltings and distortions, it can generate many descendant structures with lower

symmetry. In essence, collective excitations of  $a^0a^0c^+$  and  $a^-a^-c^0$  tilting modes in real space correspond to unstable phonon modes at the zone-boundary  $M$  point  $(1/2, 1/2, 0)$  of the  $P4/mmm$  tetragonal cell, and the antipolar modes correspond to the  $\Gamma$ -point modes at zone center  $(0, 0, 0)$  of this  $P4/mmm$  tetragonal cell. Phonon calculations are performed with the assistance of the PHONOPY code [52]. Since notable photostriction was revealed in Fig. 1(c), we take half of the well-relaxed conventional orthorhombic lattice constants at different  $n_{\text{ph}}$  as the dimension of the tetragonal cell—implying that different volumes are used for the different chosen  $n_{\text{ph}}$  in these phonon computations. We refer to the SM for more details [40].

Frequencies of relevant modes are plotted in Fig. 3. Note that there are two antipolar modes, which are dominated by La and Y ions, respectively, and the La-dominant mode is stable. Results at the dark condition are consistent with the previous study of Ref. [4] (see details in the SM [40]). Though frequencies of two  $M$ -point modes increase with  $n_{\text{ph}}$ , they are still unstable at  $n_{\text{ph}} = 1$  e/f.u. with large imaginary wave numbers. Also the increasing trend gets saturated at high  $n_{\text{ph}}$ . This also happens to the Y-dominant,  $\Gamma$ -point mode, where the frequency is saturated at  $120i$   $\text{cm}^{-1}$  when  $n_{\text{ph}} = 1$  e/f.u., while the frequency of the La-dominant,  $\Gamma$ -point mode changes only slightly under illumination.

We write down a Landau free energy model to help understand the results of these phonon calculations:

$$F = \alpha_{M_1} X_{M_1}^2 + \beta_{M_1} X_{M_1}^4 + \alpha_{M_2} X_{M_2}^2 + \beta_{M_2} X_{M_2}^4 + \alpha_{\Gamma} X_{\Gamma}^2 + \beta_{\Gamma} X_{\Gamma}^4 + \gamma X_{M_1} X_{M_2} X_{\Gamma}. \quad (4)$$

In this model,  $X$  denotes the mode amplitude, and the subscript refers to each mode. Since  $M_1^-$ ,  $M_2^-$ , and Y-dominant,  $\Gamma$ -point modes are unstable, it is necessary that their quadratic coefficients  $\alpha$  are negative, and their quartic coefficients  $\beta$  are positive. The last terms denote a trilinear coupling between three modes. Note that, in phonon calculations, the trilinear and quartic terms are not considered, as they are beyond second-order derivatives to energies within harmonic approximation. Typically, without trilinear coupling, the increasing frequency of an unstable mode denotes that the mode becomes more stable, and that will indicate a smaller tilting amplitude ( $\sqrt{|\alpha|/2\beta}$ ) with  $n_{\text{ph}}$ . However, Figs. 2(c) and 2(d) show an increase in tilting angles  $\phi$  and antipolar displacement  $\bar{D}^Y - \bar{D}^{\text{La}}$  with  $n_{\text{ph}}$ , contradicting the prediction from increasing frequencies of unstable modes. This can only be reconciled if the trilinear couplings are taken into account. Since tilting amplitudes can be approximated from the local minima of free energy  $F$  as  $X_{M_1} = |\gamma/2\alpha_{M_1}| X_{M_2} X_{\Gamma}$  and  $X_{M_2} = |\gamma/2\alpha_{M_2}| X_{M_1} X_{\Gamma}$ , we calculate the relative coupling coefficients  $\gamma/2\alpha_{M_{1,2}}$  from three mode amplitudes and plot them as a function of  $n_{\text{ph}}$  in Fig. 3(c). Anomalous behaviors of increasing tilting angles but a decreasing polarization and hardening of tilting and antipolar modes reflects the critical role light plays in tuning couplings between modes, which further modifies mode amplitudes and affects resultant polarization.

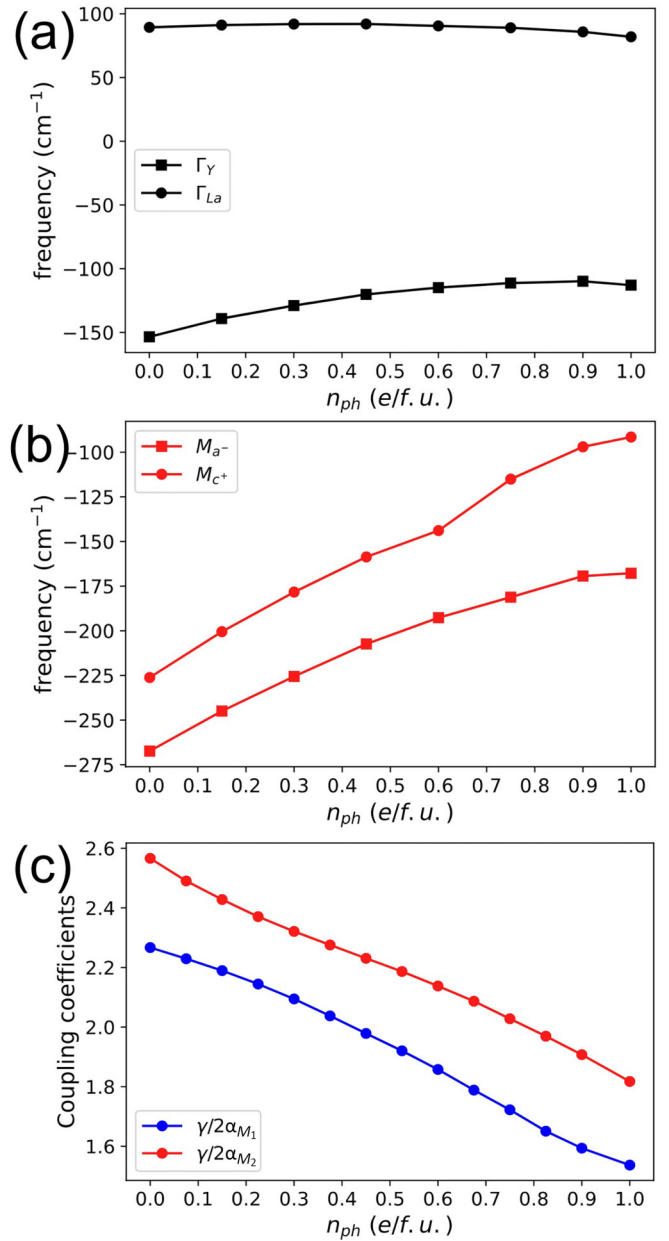


FIG. 3. Changes of phonon frequencies with  $n_{\text{ph}}$  in the parent tetragonal cell. (a) The Y-dominant and La-dominant antipolar modes at zone-center  $\Gamma$  point  $(0, 0, 0)$ . (b) Modes at zone-boundary  $M$  point  $(1/2, 1/2, 0)$  denoting  $a^-$  and  $c^+$  tiltings. (c) Changes of trilinear coupling coefficients  $\gamma/2\alpha_{M_{1,2}}$  with  $n_{\text{ph}}$  in the parent tetragonal cell.

## V. DISCUSSION

Recent experiments show how polarization can be modified with above-band-gap ultrafast light. In the ferroelectric/dielectric superlattice  $\text{PbTiO}_3/\text{SrTiO}_3$ , polarization can be rotated toward the direction normal to the surface by the ultrafast laser pulse [53]. Reduction of the in-plane and increase of the out-of-plane polarization components are due to screening of the depolarization field by the photoexcited carriers. In the  $\text{BaTiO}_3/\text{CaTiO}_3$



superlattice, lattice expansion in BaTiO<sub>3</sub> and contraction in CaTiO<sub>3</sub> is observed after the ultrafast optical excitation, indicating a polarization increase in BaTiO<sub>3</sub> but decrease in the CaTiO<sub>3</sub> layer [54]. Recently in quantum paraelectric KTaO<sub>3</sub>, a suppression of ferroelectricity is induced by photoexcitation, and has been attributed to hardening effect on transverse phonons [55]. Along with these experiments, our results indicate that hybrid-improper ferroelectrics may be an alternative system that offers new ways to optically control ferroelectric polarization. Since the present system has a relatively large band gap, the present work should also spur the search for new hybrid-improper ferroelectric systems with lower band gaps in order to be able to use visible light.

The experiments discussed above pose an intriguing question as to whether the photoinduced polarization change is an electronic or structural effect. Our calculation shows that the photoexcited thermalized carriers cause a 3.5% in-plane and a 0.6% out-of-plane lattice expansion when  $n_{\text{ph}} = 1$  e/f.u., and we wonder whether these structural effects fully account for the change of the polarization. To resolve this, we apply these strains on the lattice but under no light illumination and we then relax the internal atomic coordinates. As shown in the SM [40], in this way the total polarization decreases by 30%, which is more than twice the amount from the 12% decrease for an equal amount of strain but under illumination with  $n_{\text{ph}} = 1$  e/f.u. The different polarizations obtained in the two scenarios indicate that apart from the photostriction which deforms the lattice, the electronic effect also plays an important role in photoinduced change on polarization, which aligns energy levels of photoexcited carriers by driving intrinsic ionic displacements and therefore altering polarization. More detailed analysis about polarization from each ion with/without light can be found in the SM [40].

## VI. CONCLUSIONS

In summary, using first-principles calculations, we reveal that light can be an effective tool to manipulate ferroelectricity in hybrid-improper ferroelectric superlattices. We take the prototype system LaGaO<sub>3</sub>/YGaO<sub>3</sub> as an example and show, after photoabsorption, how polarization in the transient, quasiequilibrium state varies with the number of photoexcited thermalized carriers. A notable expansive photostriction is concomitantly observed, and the polarization change is achieved via controlling amplitudes of in-phase and out-of-phase tiltings, which are trilinearly coupled to *A*-site antipolar modes. Electronic effects associated with the occupation of thermalized carriers also contribute to the change of polarization. Recent studies show the availability to reorienting and tuning the magnitude of the polarization with the ultrafast laser pulse in ferroelectric oxides. Our study further demonstrates that (and explains why) light can be utilized as a powerful handle to govern exciting properties of functional materials in the future [55,56].

## ACKNOWLEDGMENTS

We thank Bin Xu, Hong Jian Zhao, and Peng Chen for useful discussions. L.G. and L.B. acknowledge support from MURI ETHOS Grant No. W911NF-21-2-0162 from the Army Research Office (ARO). C.P. and L.B. acknowledge ARO Grant No. W911NF-21-1-0113. L.G. acknowledges support from the Arkansas High Performance Computing Center and HPCMP for computational resources. C.P. acknowledges support from a public grant overseen by the French National Research Agency (ANR) as part of the “Investissements d’Avenir” program (Labex NanoSaclay, Reference No. ANR-10-LABX-0035) and ANR SUPERSPIN Grant No. ANR-21-CE24-0032.

- 
- [1] R. E. Cohen, Origin of ferroelectricity in perovskite oxides, *Nature (London)* **358**, 136 (1992).
  - [2] E. Bousquet, M. Dawber, N. Stucki, C. Lichtensteiger, P. Hermet, S. Gariglio, J.-M. Triscone, and P. Ghosez, Improper ferroelectricity in perovskite oxide artificial superlattices, *Nature (London)* **452**, 732 (2008).
  - [3] N. A. Benedek and C. J. Fennie, Hybrid Improper Ferroelectricity: A Mechanism for Controllable Polarization-Magnetization Coupling, *Phys. Rev. Lett.* **106**, 107204 (2011).
  - [4] J. M. Rondinelli and C. J. Fennie, Octahedral rotation-induced ferroelectricity in cation ordered perovskites, *Adv. Mater.* **24**, 1961 (2012).
  - [5] N. A. Benedek, A. T. Mulder, and C. J. Fennie, Polar octahedral rotations: A path to new multifunctional materials, *J. Solid State Chem.* **195**, 11 (2012).
  - [6] W. Zhou and A. Ariando, Review on ferroelectric/polar metals, *Jpn. J. Appl. Phys.* **59**, S10802 (2020).
  - [7] K. J. Choi, M. Biegalski, Y. Li, A. Sharan, J. Schubert, R. Uecker, P. Reiche, Y. Chen, X. Pan, V. Gopalan *et al.*, Enhancement of ferroelectricity in strained BaTiO<sub>3</sub> thin films, *Science* **306**, 1005 (2004).
  - [8] J. Haeni, P. Irvin, W. Chang, R. Uecker, P. Reiche, Y. Li, S. Choudhury, W. Tian, M. Hawley, B. Craigo *et al.*, Room-temperature ferroelectricity in strained SrTiO<sub>3</sub>, *Nature (London)* **430**, 758 (2004).
  - [9] T. Kolodiazny, M. Tachibana, H. Kawaji, J. Hwang, and E. Takayama-Muromachi, Persistence of Ferroelectricity in BaTiO<sub>3</sub> through the Insulator-Metal Transition, *Phys. Rev. Lett.* **104**, 147602 (2010).
  - [10] Y. Wang, X. Liu, J. D. Burton, S. S. Jaswal, and E. Y. Tsymlal, Ferroelectric Instability under Screened Coulomb Interactions, *Phys. Rev. Lett.* **109**, 247601 (2012).
  - [11] C. Xia, Y. Chen, and H. Chen, Coexistence of polar displacements and conduction in doped ferroelectrics: An *ab initio* comparative study, *Phys. Rev. Mater.* **3**, 054405 (2019).
  - [12] D. Hickox-Young, D. Puggioni, and J. M. Rondinelli, Persistent polar distortions from covalent interactions in doped BaTiO<sub>3</sub>, *Phys. Rev. B* **102**, 014108 (2020).
  - [13] S. Li and T. Birol, Free-Carrier-Induced Ferroelectricity in Layered Perovskites, *Phys. Rev. Lett.* **127**, 087601 (2021).
  - [14] Y. Shi, Y. Guo, X. Wang, A. J. Princep, D. Khalyavin, P. Manuel, Y. Michiue, A. Sato, K. Tsuda, S. Yu *et al.*,

- A ferroelectric-like structural transition in a metal, *Nat. Mater.* **12**, 1024 (2013).
- [15] P. W. Anderson and E. Blount, Symmetry Considerations on Martensitic Transformations: “Ferroelectric” Metals? *Phys. Rev. Lett.* **14**, 217 (1965).
- [16] Z. Fei, W. Zhao, T. A. Palomaki, B. Sun, M. K. Miller, Z. Zhao, J. Yan, X. Xu, and D. H. Cobden, Ferroelectric switching of a two-dimensional metal, *Nature (London)* **560**, 336 (2018).
- [17] A. Subedi, Proposal for ultrafast switching of ferroelectrics using midinfrared pulses, *Phys. Rev. B* **92**, 214303 (2015).
- [18] R. Mankowsky, A. von Hoegen, M. Först, and A. Cavalleri, Ultrafast Reversal of the Ferroelectric Polarization, *Phys. Rev. Lett.* **118**, 197601 (2017).
- [19] A. S. Disa, T. F. Nova, and A. Cavalleri, Engineering crystal structures with light, *Nat. Phys.* **17**, 1087 (2021).
- [20] P. Chen, C. Paillard, H. J. Zhao, J. Íñiguez, and L. Bellaiche, Deterministic control of ferroelectric polarization by ultrafast laser pulses, *Nat. Commun.* **13**, 2566 (2022).
- [21] C. Paillard, E. Torun, L. Wirtz, J. Íñiguez, and L. Bellaiche, Photoinduced Phase Transitions in Ferroelectrics, *Phys. Rev. Lett.* **123**, 087601 (2019).
- [22] V. Stoica, N. Laanait, C. Dai, Z. Hong, Y. Yuan, Z. Zhang, S. Lei, M. McCarter, A. Yadav, A. Damodaran *et al.*, Optical creation of a supercrystal with three-dimensional nanoscale periodicity, *Nat. Mater.* **18**, 377 (2019).
- [23] M. Porer, M. Fechner, E. M. Bothschafter, L. Rettig, M. Savoini, V. Esposito, J. Rittmann, M. Kubli, M. J. Neugebauer, E. Abreu *et al.*, Ultrafast Relaxation Dynamics of the Antiferrodistortive Phase in Ca Doped SrTiO<sub>3</sub>, *Phys. Rev. Lett.* **121**, 055701 (2018).
- [24] M. Porer, M. Fechner, M. Kubli, M. J. Neugebauer, S. Parchenko, V. Esposito, A. Narayan, N. A. Spaldin, R. Huber, M. Radovic, E. M. Bothschafter, J. M. Glowina, T. Sato, S. Song, S. L. Johnson, and U. Staub, Ultrafast transient increase of oxygen octahedral rotations in a perovskite, *Phys. Rev. Res.* **1**, 012005(R) (2019).
- [25] A. Kogar, A. Zong, P. E. Dolgirev, X. Shen, J. Straquadine, Y.-Q. Bie, X. Wang, T. Rohwer, I. Tung, Y. Yang *et al.*, Light-induced charge density wave in LaTe<sub>3</sub>, *Nat. Phys.* **16**, 159 (2020).
- [26] G. Marini and M. Calandra, Light-Tunable Charge Density Wave Orders in MoTe<sub>2</sub> and WTe<sub>2</sub> Single Layers, *Phys. Rev. Lett.* **127**, 257401 (2021).
- [27] C. Paillard, B. Xu, B. Dkhil, G. Geneste, and L. Bellaiche, Photostriction in Ferroelectrics from Density Functional Theory, *Phys. Rev. Lett.* **116**, 247401 (2016).
- [28] C. Paillard, S. Prosandeev, and L. Bellaiche, *Ab initio* approach to photostriction in classical ferroelectric materials, *Phys. Rev. B* **96**, 045205 (2017).
- [29] R. Haleoot, C. Paillard, T. P. Kaloni, M. Mehboudi, B. Xu, L. Bellaiche, and S. Barraza-Lopez, Photostrictive Two-Dimensional Materials in the Monochalcogenide Family, *Phys. Rev. Lett.* **118**, 227401 (2017).
- [30] S. Sarkar, I.-W. Un, Y. Sivan, and Y. Dubi, Theory of non-equilibrium ‘hot’ carriers in direct band-gap semiconductors under continuous illumination, *New J. Phys.* **24**, 053008 (2022).
- [31] J. Fast, U. Aeberhard, S. P. Bremner, and H. Linke, Hot-carrier optoelectronic devices based on semiconductor nanowires, *Appl. Phys. Rev.* **8**, 021309 (2021).
- [32] A. Othonos, Probing ultrafast carrier and phonon dynamics in semiconductors, *J. Appl. Phys.* **83**, 1789 (1998).
- [33] D. König, K. Casalenuovo, Y. Takeda, G. Conibeer, J. Guillemoles, R. Patterson, L. Huang, and M. Green, Hot carrier solar cells: Principles, materials and design, *Physica E* **42**, 2862 (2010).
- [34] A. R. Attar, H.-T. Chang, A. Britz, X. Zhang, M.-F. Lin, A. Krishnamoorthy, T. Linker, D. Fritz, D. M. Neumark, R. K. Kalia *et al.*, Simultaneous observation of carrier-specific redistribution and coherent lattice dynamics in 2H-MoTe<sub>2</sub> with femtosecond core-level spectroscopy, *ACS Nano* **14**, 15829 (2020).
- [35] D. M. Fritz, D. Reis, B. Adams, R. Akre, J. Arthur, C. Blome, P. Bucksbaum, A. L. Cavalieri, S. Engemann, S. Fahy *et al.*, Ultrafast bond softening in bismuth: Mapping a solid’s interatomic potential with X-rays, *Science* **315**, 633 (2007).
- [36] E. G. Gamaly, The physics of ultra-short laser interaction with solids at non-relativistic intensities, *Phys. Rep.* **508**, 91 (2011).
- [37] H. Yasuda, Y. Yamada, T. Tayagaki, and Y. Kanemitsu, Spatial distribution of carriers in SrTiO<sub>3</sub> revealed by photoluminescence dynamics measurements, *Phys. Rev. B* **78**, 233202 (2008).
- [38] P. Tangney and S. Fahy, Calculations of the A<sub>1</sub> Phonon Frequency in Photoexcited Tellurium, *Phys. Rev. Lett.* **82**, 4340 (1999).
- [39] E. D. Murray, D. M. Fritz, J. K. Wahlstrand, S. Fahy, and D. A. Reis, Effect of lattice anharmonicity on high-amplitude phonon dynamics in photoexcited bismuth, *Phys. Rev. B* **72**, 060301(R) (2005).
- [40] See Supplemental Material at <http://link.aps.org/supplemental/10.1103/PhysRevB.107.104109> for computational methods, density of states, phonon calculation, and polarization under strain without light illumination.
- [41] J. P. Perdew and A. Zunger, Self-interaction correction to density-functional approximations for many-electron systems, *Phys. Rev. B* **23**, 5048 (1981).
- [42] P. E. Blöchl, Projector augmented-wave method, *Phys. Rev. B* **50**, 17953 (1994).
- [43] D. M. Ceperley and B. J. Alder, Ground State of the Electron Gas by a Stochastic Method, *Phys. Rev. Lett.* **45**, 566 (1980).
- [44] A. M. Glazer, The classification of tilted octahedra in perovskites, *Acta Crystallogr., Sect. B: Struct. Crystallogr. Cryst. Chem.* **28**, 3384 (1972).
- [45] X. Gonze, B. Amadon, P.-M. Anglade, J.-M. Beuken, F. Bottin, P. Boulanger, F. Bruneval, D. Caliste, R. Caracas, M. Côté *et al.*, ABINIT: First-principles approach to material and nanosystem properties, *Comput. Phys. Commun.* **180**, 2582 (2009).
- [46] B. Peng, D. Bennett, I. Bravić, and B. Monserrat, Tunable photostriction of halide perovskites through energy dependent photoexcitation, *Phys. Rev. Mater.* **6**, L082401 (2022).
- [47] C. Paillard and L. Bellaiche, Light: A new handle to control the structure of cesium lead iodide, *Phys. Rev. B* **107**, 054107 (2023).
- [48] A. Narayan, Effect of strain and doping on the polar metal phase in LiOsO<sub>3</sub>, *J. Phys.: Condens. Matter* **32**, 125501 (2020).
- [49] A. T. Mulder, N. A. Benedek, J. M. Rondinelli, and C. J. Fennie, Turning ABO<sub>3</sub> antiferroelectrics into ferroelectrics: Design rules for practical rotation-driven ferroelectricity in double

- perovskites and  $A_3B_2O_7$  Ruddlesden-Popper compounds, *Adv. Funct. Mater.* **23**, 4810 (2013).
- [50] H. J. Zhao, J. Iniguez, W. Ren, X. M. Chen, and L. Bellaiche, Atomistic theory of hybrid improper ferroelectricity in perovskites, *Phys. Rev. B* **89**, 174101 (2014).
- [51] L. Bellaiche and J. Iniguez, Universal collaborative couplings between oxygen-octahedral rotations and antiferroelectric distortions in perovskites, *Phys. Rev. B* **88**, 014104 (2013).
- [52] A. Togo and I. Tanaka, First principles phonon calculations in materials science, *Scr. Mater.* **108**, 1 (2015).
- [53] H. J. Lee, Y. Ahn, S. D. Marks, E. C. Landahl, S. Zhuang, M. H. Yusuf, M. Dawber, J. Y. Lee, T. Y. Kim, S. Unithrattil *et al.*, Structural Evidence for Ultrafast Polarization Rotation in Ferroelectric/Dielectric Superlattice Nanodomains, *Phys. Rev. X* **11**, 031031 (2021).
- [54] D. Sri Gyan, H. J. Lee, Y. Ahn, R. B. Carson, J. Carnis, T. Y. Kim, S. Unithrattil, J. Y. Lee, S. H. Chun, S. Kim *et al.*, Optically induced picosecond lattice compression in the dielectric component of a strongly coupled ferroelectric/dielectric superlattice, *Adv. Electron. Mater.* **8**, 2101051 (2022).
- [55] V. Krapivin, M. Gu, D. Hickox-Young, S. W. Teitelbaum, Y. Huang, G. de la Peña, D. Zhu, N. Sirica, M.-C. Lee, R. P. Prasankumar, A. A. Maznev, K. A. Nelson, M. Chollet, J. M. Rondinelli, D. A. Reis, and M. Trigo, Ultrafast Suppression of the Ferroelectric Instability in  $\text{KTaO}_3$ , *Phys. Rev. Lett.* **129**, 127601 (2022).
- [56] C. Song, Q. Yang, X. Liu, H. Zhao, C. Zhang, and S. Meng, Electronic origin of laser-induced ferroelectricity in  $\text{SrTiO}_3$ , *J. Phys. Chem. Lett.* **14**, 576 (2023).